Journal of Molecular Modeling (2021) 27: 55
https://doi.org/10.1007/s00894-020-04661-5

ORIGINAL PAPER

Effectiveness of coarse graining degree and speedup on the dynamic properties of homopolymer

Lijuan Liao[1] · Changyu Meng[1,2] · Chenguang Huang[1,2]

Received: 26 August 2020 / Accepted: 20 December 2020 / Published online: 28 January 2021
© The Author(s), under exclusive licence to Springer-Verlag GmbH, DE part of Springer Nature 2021

Abstract

Evaluation of effective coarse graining (CG) degree and reasonable speedup relative to all-atomistic (AA) model was conducted to provide a basis for building appropriate larger-scale model. The reproducibility of atomistic conformation and temperature transferability both act as the analysis criteria to resolve the maximum acceptable CG degree. Taking short- and long time spans into account simultaneously in the estimation of computational speedup, a dynamic scaling factor is accessible in fitting mean squared displacement ratio of CG to AA as an exponential function. Computing loss in parallel running is an indispensable component in acceleration, which was also added in the evaluation. Subsequently, a quantified prediction of CG speedup arises as a multiplication of dynamic scaling factor, computing loss, time step, and the square of reduction in the number of degrees of freedom. Polyethylene oxide was adopted as a reference system to execute the direct Boltzmann inversion and iterative Boltzmann inversion. Bonded and non-bonded potentials were calculated in CG models with 1~4 monomers per bead. The effective CG degree was determined as two at the most with a speedup of four orders magnitude over AA in this study. Determination of effectiveness CG degree and the corresponding speedup prediction provide available tools in larger spatiotemporal-scale calculations.

Keywords Coarse graining (CG) degree · Speedup · Iterative Boltzmann inversion (IBI) · Temperature transferability · Dynamic behavior

Introduction

With complex chain or crosslink structures and dynamic mechanical behaviors, polymer exhibits multi-scale characteristics. However, whether top-down or bottom-up approach incorporating various space-time scales is still a big challenge in polymeric materials [1]. An effective multi-scale modelling technique is indispensable to clarify the relationship of microstructure and macro-mechanical performance.

✉ Lijuan Liao
liaohuanxin@hotmail.com

[1] Key Laboratory for Mechanics in Fluid Solid Coupling Systems, Institute of Mechanics, Chinese Academy of Sciences, No.15, Beisihuan West Road, Haidian District, Beijing 100190, People's Republic of China

[2] School of Engineering Science, University of Chinese Academy of Sciences, No.19(A), Yuquan Road, Shijingshan District, Beijing 100049, China

As a parameterized meso-scale simulation method, systematic coarse-graining (CG) method integrates a monomer unit into one pseudo-atomic bead. It constructs the CG bead interactions to match the structural distribution function calculated by atomistic simulations. The concept of CG depends on both time and length scale separation of fast and slow variables of the system [2]. Since fewer interacting sites are required in modeling, shorter range and softer interactions should be calculated effectively with larger integration time step [3]. With several orders of magnitude higher in efficiency than atomistic simulations, systematic CG method can be used to accelerate the simulation of the network structure of polymers.

Recently, swarm optimization [4], machine learning approach [5], and iterative Boltzmann inversion (IBI) [6] have attracted attention as representative CG methods to extend spatiotemporal scales. Among them, as a typical systematic CG method, IBI matches the atomistic structures to obtain potential functions. The structure of CG skin ceramides [7] and the self-assembly behavior of a monolayer film on gold [8] were successfully described by the IBI method. Primitive chain network of un- and crosslinked cis-polyisoprene (PI)

polymer were analyzed by CG molecular dynamics (MD) simulation [9]. Viscoelastic properties of PI were also calculated by the IBI method. In addition, different bridging laws, i.e., CGMD method, primitive path analysis, and the affine-deformation assumption, were applied to scale up from nano to meso, meso to micro, and micro to macro [10]. A CG potential for di-block copolymer poly (styrene-*b*-butadiene) was provided to test static and dynamic properties effectively [11]. The inter-chain potentials of the CG model for polycarbonates were obtained by Boltzmann inversion [12]. Inter-bead potentials, equivalent of bonded potential in all-atomistic (AA) model, were calculated by simple iterative computation for PI both in liquid and melt [6].

Viscoelastic dynamic responses of polymers, which are profoundly interrelated with chain and network structures, are vital to the macro- mechanical behaviors. Accordingly, the IBI method is an appropriate approach to match the microstructure parameters, and then to examine the dynamic mechanical behaviors. Corrections are necessary to improve the state transferability, such as pressure and temperature optimizations [13, 14]. There are still problems such as undermined effective CG degree and unreasonable prediction of acceleration of the dynamic behavior of polymer systems [15], even though the systematic CG method has been developed for several years.

How to define the number of atoms or monomers in a single pseudo-atomic bead is of great significance to measure the capability of the CG model in capturing the static and dynamic properties of AA one. One representative attempt [16] was carried out depending on the analysis of plateau modulus, mean squared displacement (MSD), and density variation with respect to the temperature taking polyethylene (PE) as the model. They [17] demonstrated the potential capability of CG models in capturing polymeric motions even reaching hundreds of microseconds. These works provide a useful concept in extending the time and length scales in simulation. However, more details should be explored to apply it to practice with sufficient convenience.

Another issue of concern for CG is the acceleration in calculation. The mechanism of speedup for CG was described in detail [18, 19], which brings a theoretical estimation of speedup including contributions from the scale factor, time step, and the reduction in the number of pairwise interactions [16]. However, the obtaining of scale factor lies on the matching target atomistic MSD on a long-time scale. Computing cost and matching strategy for scaling constant should be considered. Moreover, the existing theoretical estimation of speedup is ideal without considering the computing loss in parallel running, which may lead the overestimation.

Aiming to establish a useful evaluation of effective CG degree and the corresponding speedup in dynamic calculations, the two issues mentioned above are addressed with the help of CG simulation on the static and dynamic properties of polyethylene oxide (PEO). Some works of CG models about PEO by MARTINI CG force field [20, 21] or IBI [22] were reported, which provided the reference material properties in CG simulations representatively. The adopted CG method here includes the calculations of CG bonded and non-bonded potentials, where the former refers to the direct Boltzmann inversion (DBI) and the latter is defined as parameterized CG to reproduce the target properties in atomistic simulations [23]. Consisting of identical monomer units, the results obtained in this study are assumed to possess a good expansibility to other types of homopolymer.

The article is organized as follows. In the "Simulation details" section, the simulation details are described, including the parameter sensitivity analysis and the obtaining of CG potentials. The static and dynamic properties are captured by AA and CG models, which are used to evaluate the effective CG degree and the corresponding speedup in the "PEO property analysis" section. Finally, the discussion is provided and conclusions are summarized.

Simulation details

PEO systems with different chain lengths were denoted as PEO-n, where n is the number of monomers -[-CH_2-O-CH_2-]- [24] in a single chain. The CG degree λ was defined as the number of monomers in a single pseudo-atomic bead (referring to these models as CG-λ). Taking an example, a single PEO-60 chain of AA and CG models with 1~4 CG degree are illustrated in Fig. 1, where 422 atoms, 60 beads, 30 beads, 20 beads, and 15 beads are included in each model, respectively.

Chains of PEO were thrown randomly into a periodic cubic-box via Packmol [25] with a relatively low density approximately 0.154 g·cm^{-3} initially. After minimization, the relaxation of each atomistic model was carried out in the NPT ensemble with T = 500 K and P = 1 atm for 2 ns firstly. Sequentially, each system experiences a cooling process to room temperature (T_r) with a rate of 0.2 K·ps^{-1} lasting for 1 ns. Further NPT relaxation was performed at T_r for 1 ns. As for different target temperatures (T_t), each system was heated from T_r to T_t in the NVT ensemble for 1 ns. A long relaxation in the NPT ensemble was performed for 50 ns at T_t, which exceeds the rotational or diffusional relaxation time [26]. The examination on the effect of cooling rate was performed in Figure S1 in Supplementary Material, which shows that the value of 0.2 K·ps^{-1} as the cooling rate can be acceptable in deriving CG potentials.

The trajectories in the final 1-ns relaxation in the NVT ensemble were captured as the target distribution functions to parameterize the CG potentials. Time step Δt is 1 fs in atomistic simulations.

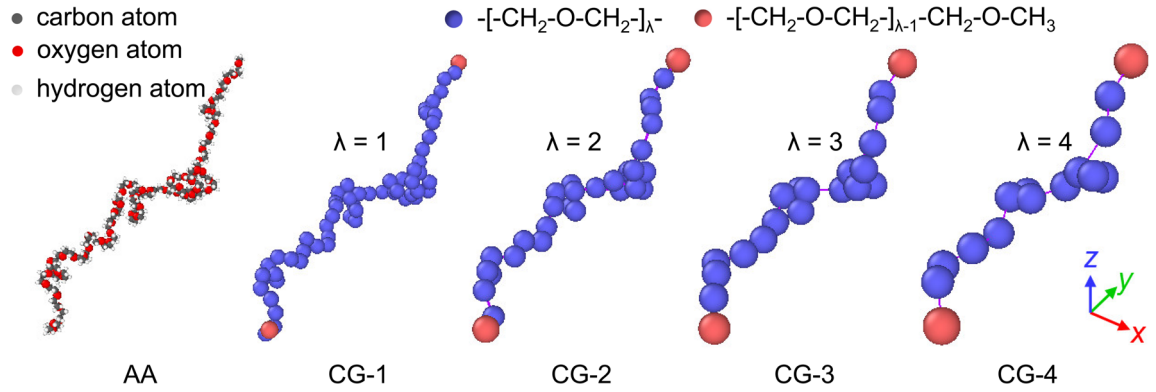

Fig. 1 A single PEO-60 chain represented with increasing CG degree

Each CG potential component was obtained by DBI (bonded part) and IBI (non-bonded part) from each target distribution function of the atomistic model. The factor for potential robustness was set as 0.05 [26] to improve the convergence and stability of the IBI process. A pressure correction was applied to match the density at equilibrium, where the scaling factors were set as 3.0×10^{-4} for CG-1~2 and 5.0×10^{-3} for CG-3~4 in a simple pressure correction method [6]. IBI procedure implemented here leads to converged RDFs of non-bonded interactions within 300 iterations. The corresponding convergence coefficient ranges from 0.15 to 2.50 as CG degree increases. The averaged pressure converges to the target pressure 1 atm after iteration. The time step Δt was set as 10 fs during the IBI process and CG calculations. In Figure S2 in Supplementary Material, evolutions of convergence coefficient and system pressure during iteration by IBI taking CG-1 as an example were provided. The analysis provides evidence that all these parameters during the IBI procedure were suitable for the calculations in this study.

Both DBI and IBI procedures should be carried out in each target temperature. According to the mapping CG topology and potentials, the dynamic behaviors are possibly examined in higher spatiotemporal scale relative to the atomistic scale. MD runs and IBI procedures were implemented using LAMMPS [27] and VOTCA [28], respectively. Visualizations employ VMD [29] and OVITO [30].

Parameter sensitivity analysis

The interaction potential is essential in MD calculations to reproduce the intrinsic properties reasonably. For atomistic PEO, potentials like the united atom (UA) [18, 31, 32], OPLS-AA [33–35], Charmm-AA [20], Smith [36, 37], and TraPPE-UA [38–40] were previously used to examine the properties of the bulk, melt, and in solution, respectively. The simplest PEO-4 model (two monomers and two end groups) at T_t = 500 K in the melt was adopted as an example of the sensitivity analysis of the CG parameters. For the atomistic potentials, we consider the OPLS-AA and TraPPE-UA models. The averaged densities at T_r of PEO-4 with 500 chains at equilibrium from three samples are 0.97 g·cm^{-3} by OPLS-AA and 1.03 g·cm^{-3} by TraPPE-UA, respectively. Both are close to the experimental measurement 0.986 g·cm^{-3} [20].

CG mapping largely depends on the location of CG bead center [10]. Two common definitions of CG-1 bead center for PEO are the center of monomer mass [20, 32, 33, 35] (denoted as c.m.) and the center of oxygen atom [18, 36] (denoted as c.o.). Their effects on the CG mapping and CG potentials were both discussed here.

The transferability of chain length was also considered, where n = 4 and 60 were chosen. With the similar initial density in each box with side-length 100 Å before relaxation, the chain numbers of PEO-4 and PEO-60 are 500 and 35, respectively. Two more models with chain lengths as 18 and 50 were also examined to discuss the dependence of chain length. The comparisons can be referred in Figure S3 in Supplementary Material.

As illustrated in Fig. 2, each CG potential component obviously depends on the atomistic potential and mapping center of CG bead (data marked as red open square and blue open circle). The patterns of the obtained CG potentials marked as black open square present good agreement compared with the results reported in the literature [35]. The difference from the chain length is almost immeasurably as illustrated in Fig. 2 (comparison between the data marked as black open square and olive multiplication sign), which suggests that the accuracy of CG potentials is independent on the chain length. Figure S3 in Supplementary Material further proves this conclusion. This provides an effective approach to get CG potentials of PEO with longer chains by iterations according to the counterpart with shorter ones. Enormous numbers of monomers ranging from hundreds to thousands in a single PEO chain in practice, a model with chain length n = 60 (as the common multiple of 1, 2, 3, and 4) was taken as the representative system in the current study, which is convenient for discussing the effectiveness of CG degree and evaluating the corresponding speedup as following.

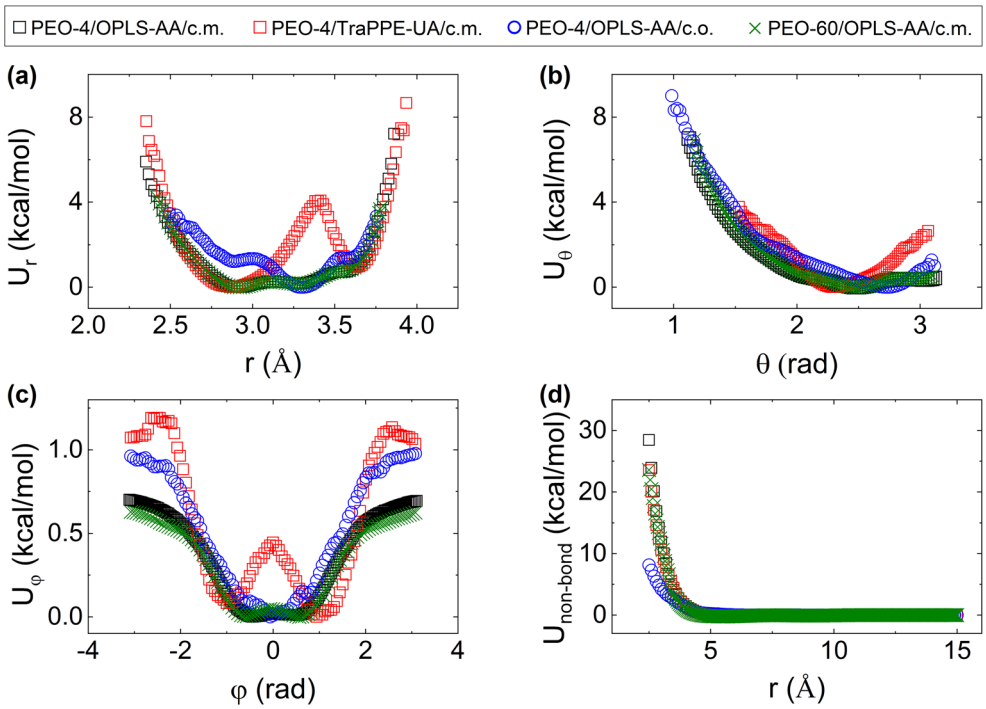

Fig. 2 Analysis of parameter sensitivity on mapping and potential component of CG-1 at 500 K, **a** bond, **b** angle, **c** dihedral angle, and **d** non-bond.

Coarse graining potential calculation

According to the above analysis, OPLS-AA and c.m. were selected as atomistic potential and mapping bead center in the following, which are also supported by the studies on PEO in melt [20, 32, 33]. For simplicity, identical CG bead interaction was defined even though with a difference hydrogen atom mass between middle and end CG beads.

Each CG potential component was obtained as shown in Fig. 3 taking CG-1 at 500 K as an example. Harmonic functions for bond $U_b(r) = k_b(r\text{-}r_0)^2$ and three-body angle $U_a(\theta) = k_a(\theta\text{-}\theta_0)^2$, and multi-harmonic function for dihedral torsion $U_\varphi(\varphi) = \Sigma k_i \cos^{i-1}(\varphi)$ (i = 1~5) were employed to fit the corresponding tabulated forms, respectively. The fitted curves were plotted to reproduce the DBI potential distributions of CG bond, angle, and dihedral angle as plotted in Fig. 3a–c

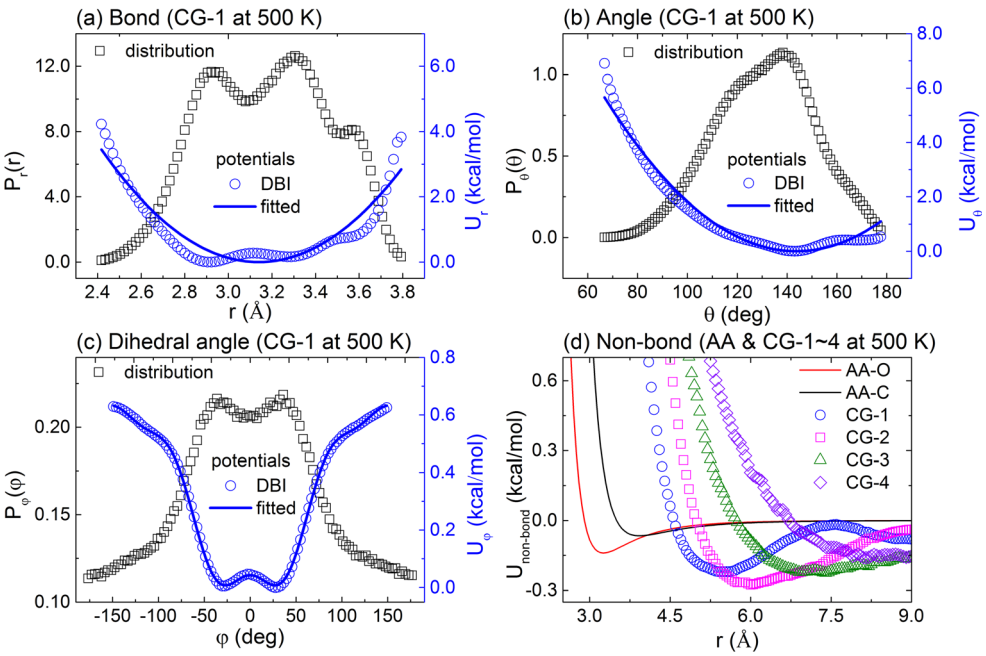

Fig. 3 Structural distributions, DBI, and fitted potentials and IBI potential at 500 K, **a** bond of CG-1, **b** angle of CG-1, **c** dihedral angle of CG-1, and **d** optimized non-bond potentials of CG-1~4.

with a reasonable approximation. Pearson correlation coefficients are 95.3% for bond, 98.7% for angle, and 99.9% for dihedral angle, respectively. Rather than the Lennard-Jones (LJ) form, tabulated potentials were adopted for CG nonbonded part for accuracy, and these curves of examples are summarized in Fig. 3d. The atomistic pair potentials of oxygen atom (AA-O) and carbon atom (AA-C) are included for comparison. A suggestion from mapping AA models onto CG models was introduced as that a single CG bond represents about four to five carbon-carbon backbone bonds [41]. Similarly, the dihedral component was considered implicitly in CG-3 (a bead with eight backbone bonds) and CG-4 (a bead with eleven backbone bonds) systems. All the parameters of bonded potential components in discussed cases are summarized in Table S1 of Supplementary Material.

PEO property analysis

Static analysis

The end-to-end distance R_{ee} and the radii of gyration R_g of chains were used to characterize the static behaviors. Following the Gaussian distributions as shown in Fig. 4a–f, the example CG model predicts both R_{ee} and R_g well, which provides much higher agreement with atomistic calculations than that described in previous work [35]. Probably, the nonbonded potential form causes the differences in capturing the structural properties, where the tabulated potentials were used here in comparing with the shifted LJ 12-6 ones with a smooth function in literature [35]. The expectation of each Gaussian distribution was denoted as μ. As plotted in Fig. 4g taking T_t = 500 K as an example, the increase of CG degree λ brings lower expectation μ both for R_{ee} [16] and R_g. However, the subtle change of R_g is only 7.4% from AA to CG-4. The ratio $(R_{ee}/R_g)^2$ estimates the conformation of a chain with a reference value of 6 [42]. As described in Fig. 4h, the values of $(R_{ee}/R_g)^2$ at 500 K (AA: 6.72, CG-1: 6.87) and 400 K (AA: 5.86, CG-1: 5.48) are close to those reported in the literature [35] (AA: 6.46 and CG-1: 6.86 at 500 K, AA: 5.38 and CG-1: 5.41 at 423 K, AA: 5.47 and CG-1: 5.48 at 363 K), respectively. Combing Fig. 4g with Fig. 4h, as CG degree λ increases and temperature decreases, the chains evolve from elongated conformation to compact conformation. In addition, as shown in Fig. 4i, smaller values of both R_{ee} and R_g in chains can be observed at lower temperature, which agrees well with the existing results [43].

Temperature transferability analysis

AA and CG-λ (λ = 1~4) systems were cooled from 500 to 100 K with a rate of 20 K·ns^{-1}. Notably, the CG potentials were used with the parameters at 500 K obtained by DBI and IBI to examine the temperature transferability.

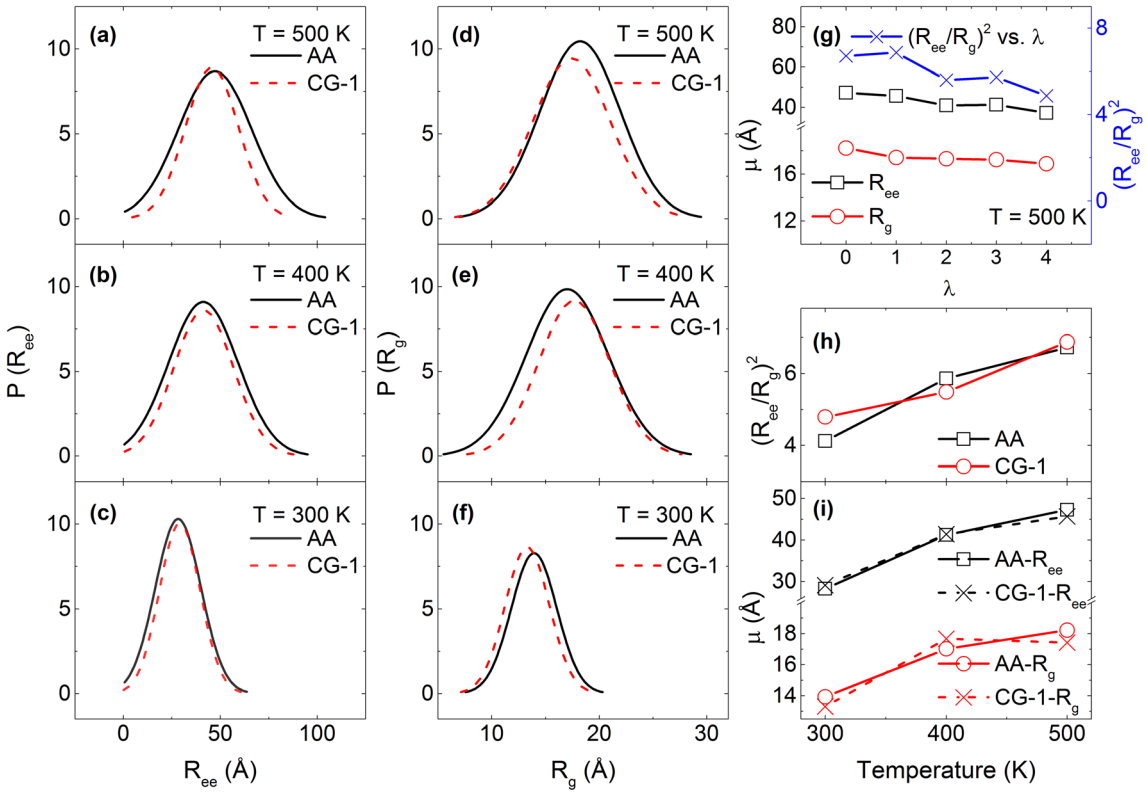

Fig. 4 Distributions and variations with respect to the CG degree and temperature of R_{ee} and R_g

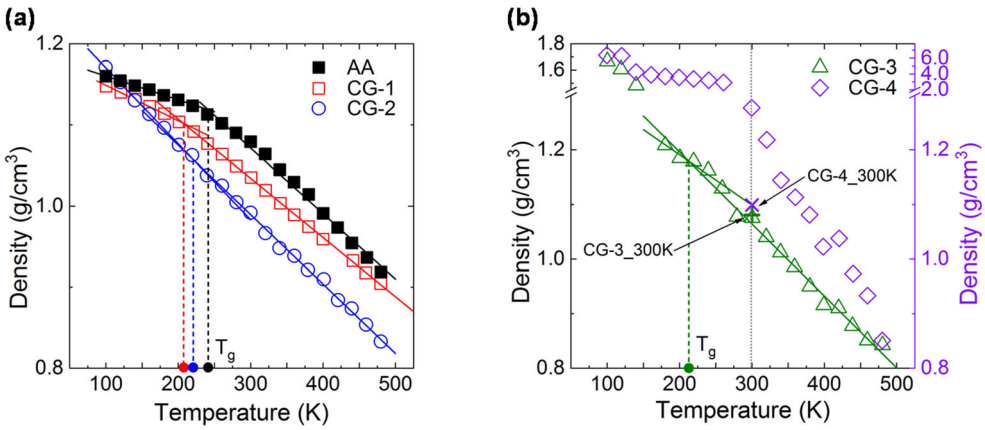

Fig. 5 Density versus temperature for AA and CG-λ (λ = 1-4) models cooling from 500 to 100 K with a rate of 20 K/ns. For each CG model, the potentials were obtained at 500 K in melt. In subplot (**b**), the data marked as olive cross and violet multiplication sign were calculated at 300 K.

As illustrated in Fig. 5, the density of each system climbs during cooling. The values of PEO density were provided by the literature [43] as 1.127 g·cm^{-3} at 298 K, 1.038 g·cm^{-3} at 413 K, and 0.976 g·cm^{-3} at 493 K, respectively. The developed CG potentials for λ = 1, 2 show excellent temperature transferability. However, well temperature transferability of λ = 3 and λ = 4 can be observed only in the range of T > 160 K and T > 400 K, respectively. As a reference, the average equilibrium density of CG-3 obtained by CG potentials at 300 K was marked as an olive cross. It agrees well with the upper triangle at 300 K during cooling, which provides evidence of temperature transferability of CG-3 at least in the range of 500 to 300 K. However, using the CG-4 potentials obtained at 300 K, the average equilibrium density is 1.099 g·cm^{-3}, which is close to that of the atomistic model. The counterpart during cooling is far from the violet cross. The CG-4 potentials lose the temperature transferability gradually for T < 400 K. Referring to the potential parameters in Table S1, softer bond and angle potentials were obtained at lower temperature for λ = 3, 4. In addition, CG creates a smoother free-energy landscape and less frictional forces [16, 44]. It is evident that the compressibility of the system with high CG degree is greatly enhanced. CG-3 and CG-4 show the improved compressibility by cooling as plotted in Fig. 5b. The melting temperature T_m of PEO was reported as 340 K [45]. A sharp rise of CG-4 density occurs in the range of 260–320 K, which is assumed as the indicator of semi-crystalline. Returning to Fig. 3d, a larger equilibrium bond distance was obtained in a higher CG degree during mapping.

Some studies suggested that a modified soft segment repulsive potential should be imposed between CG beads to prevent unphysical bond crossings [16, 46, 47]. It can be assumed that the standard IBI is not enough to capture the reasonable potential parameters as CG degree increases with softer potentials, smoother energy landscape, and less frictional forces.

The cross point of two fitting lines of glassy and rubbery states indicates the glass-transition temperature (T_g). Referred to T_g reported as 190–210 K [48], 208 K [45], and 203–204 K [43], the values as predicted in Figure 5 are acceptable as 241.21 K for AA model, 206.74 K for CG-1 model, 220.37 K for CG-2 model and 212.29 K for CG-3 model, respectively. With well temperature transferability, CG-1 and CG-2 model are capable of reasonably predicting T_g.

Dynamic analysis

MSD at 500 K was analyzed to examine the dynamic behaviors of AA and CG models. CG-1~2 models were considered according to the good temperature transferability discussed in the above section.

Resulting from lower activation energy [35], the model with a higher CG degree moves faster, as shown in Fig. 6a. The two CG models collapse onto the atomistic curve by scaling factors [16, 18, 19, 49] to extend the temporal range as an accelerated strategy. The target diffusion coefficient (denoted as D) was predicted by MSD linearly fitting as 3.4 × 10^{-6} cm^2·s^{-1}, which agrees well with the interpolating value listed in the literature [43]. Accordingly, the time scaling factors of CG-1 and CG-2 were obtained by matching D as 5.8 and 13.8, respectively, as plotted in Fig. 6b with scaled time ranges t^*.

However, a constant scaling factor related to the ratio of self-diffusivities was reported insufficient in the literature [26]. They hold an opinion that the governing factors of self-diffusion evolve from the available thermal energy and atomic momenta to the frictional forces gradually. This point comes from the temporal ratio of MSD from CG and AA, which increases to an asymptotic value rather than a constant [26, 35]. The time-dependent variation of ratio was fitted by exponential form as $1 + \beta\,[1 - \exp(-t \cdot \tau^{-1})]$, where β and τ indicate the dynamic scaling factor and transition time, respectively.

As fitted in Fig. 6c, the obtained dynamic scaling factors of MSD ratio from CG-1 over AA (CG-1/AA) and CG-2 over AA (CG-2/AA) are 6.5 and 14.0, respectively. The transition times for CG-1/AA and CG-2/AA are 37.5 ns and 43.5 ns, respectively. The scaling factors obtained by time scaling to match D (5.8 for CG-1 to AA and 13.8 for CG-2 to AA) coincide with the counterparts by MSD ratio fitting (6.5 for CG-1 to AA and 14.0 for CG-2 to AA), even with different

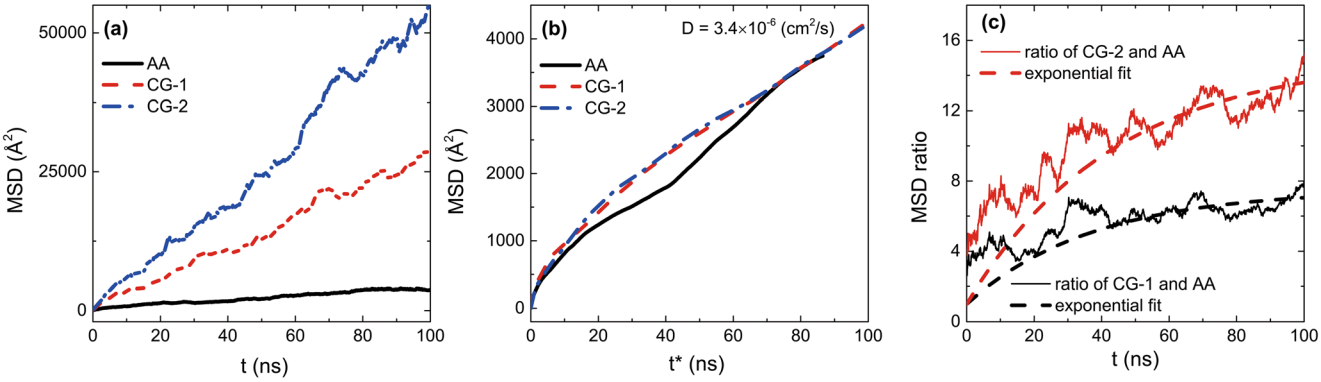

Fig. 6 Diffusion behaviors and dynamic scaling factor examination at 500 K. **a** MSD of AA and CG-1~2 models. **b** MSD of AA model and time-scaled MSD of CG-1~2. **c** MSD ratios of CG to AA and exponential fits

physical meanings. Correspondingly, the speedup of CG-2 over CG-1 is 2.4 (13.8/5.8) by time scaling and 2.2 (14.0/6.5) by MSD ratio fitting, which agrees well with each other. The factor β is an indicator of scaling constant in long time scale, which expands the physical meaning of scaling constant taking short and long-time spans into account. Accordingly, as a dynamic scaling factor, β is more suitable to characterize the dynamic acceleration in practice with higher convenience.

Discussion and conclusions

With less degrees of freedom, CG calculations were used to extend time and length scales. A model with an effective CG degree should have the ability to capture the atomistic behaviors reasonably within longer time and length scales. In this work, conformation microstructures were described well by CG models. Combing with temperature effect and self-diffusivity, the maximum acceptable CG degree to correctly describe microscopic behavior and properties via standard IBI is $\lambda = 2$, where one CG bond represents five backbone bonds. Hence, a CG model with fourteen atoms as a bead (fifteen atoms as a terminal bead) reproduces the conformational and diffusional behaviors effectively with well temperature transferability in the range of 100 to 500 K for PEO. The obtained effective CG degree was supported by the empirical suggestion in CG modeling [41], where a CG bond represents about four to five carbon-carbon backbone bonds during mapping AA models onto CG ones.

Another important reason for developing CG algorithm is speedup in calculation. Three aspects [16] contribute to the speedup in CG, as dynamic scaling factor β, CG time step Δt and reduction in the number of degrees of freedom 3λ. Accordingly, the theoretical speedup is the multiplication of the above three parties, as $\beta \times \Delta t \times (3\lambda)^2$. Thus, the speedup of CG-1 and CG-2 over AA calculations reaches five and six orders of magnitude. In practical, the consumption of interactive data between nodes in parallel running and additional occupation should be considered. Taking an example, atomistic PEO with 15 k atoms in NVT assemble run in parallel on 48 cores at a rate of 20.4 ns per day, while equivalent CG-1 and CG-2 calculated at 1.8 μs and 5.5 μs per day on 24 cores, respectively. Speedups of four and three orders of magnitudes of CG-1 and CG-2 relative to AA were evaluated, respectively. An appropriate loss factor should be considered in evaluation speedup taking CPU performance, engaging core, etc. into account. This estimation to the case provided in ref. [26] is also suitable, where the listed computational occupation matches the predicted magnitude order.

Here, the standard IBI was chosen to examine the performance of CG models. After correction of RDF and pressure in iteration, CG models present the equivalent static properties of the atomistic model. Referring to the variation of density with respect to temperature, effective CG degree was identified. This helps to build an appropriate CG model to balance the accuracy and effectiveness in the calculation. In addition, an evaluation of speedup was improved as the multiplication of dynamic scaling factor, computing loss factor, time step, and the square of reduction in the number of degrees of freedom. The establishment of effective CG degree determination and quantified speedup prediction provides a useful tool to evaluate the larger spatiotemporal-scale calculations and select appropriate CG strategy in practice. Finally, it is possible to improve the maximum acceptable CG degree with the help of modification on CG pair potential to inhibit unphysical bond crossings and correction on frictional and stochastic forces.

Supplementary Information The online version contains supplementary material available at https://doi.org/10.1007/s00894-020-04661-5.

Acknowledgments The parallel computing was supported by the National Supercomputing Center in Shenzhen (Shenzhen Cloud Computing Center) and the Computing Facility, Institute of Mechanics, Chinese Academy of Sciences.

Authors' contributions Conceptualization: Lijuan Liao; Methodology: Lijuan Liao and Changyu Meng; Formal analysis and investigation: Lijuan Liao and Changyu Meng; Writing—original draft preparation: Lijuan Liao; Funding acquisition: Lijuan Liao; Supervision: Chenguang Huang.

Funding This study was funded by the National Natural Science Foundation of China (Project No. 11672314).

Data availability N/A.

Compliance with ethical standards

Conflict of interest The authors declare that they have no conflict of interest.

Ethics approval N/A.

Consent to participate N/A.

Consent for publication N/A.

Code availability N/A.

References

1. Gooneie A, Schuschnigg S, Holzer C (2017) A review of multiscale computational methods in polymeric materials. Polymers 9(1):1–80. https://doi.org/10.3390/polym9010016
2. Ohkuma T, Kremer K (2017) Comparison of two coarse-grained models of cis-polyisoprene with and without pressure correction. Polymer 130:88–101. https://doi.org/10.1016/j.polymer.2017.09.062
3. Noid WG (2013) Systematic methods for structurally consistent coarse-grained models. In: Monticelli L, Salonen E (eds) Biomolecular Simulations: Methods and Protocols. Humana Press, Totowa, pp 487–531. https://doi.org/10.1007/978-1-62703-017-5_19
4. Empereur-mot C, Pesce L, Bochicchio D, Perego C, Pavan GM (2020) Swarm-CG: Automatic parametrization of bonded terms in coarse-grained models of simple to complex molecules via fuzzy self-tuning particle swarm optimization. ChemRxiv. https://doi.org/10.26434/chemrxiv.12613427.v2
5. Bejagam KK, Singh S, An Y, Deshmukh SA (2018) Machine-learned coarse-grained models. J Phys Chem Lett 9(16):4667–4672. https://doi.org/10.1021/acs.jpclett.8b01416
6. Reith D, Putz M, Muller-Plathe F (2003) Deriving effective mesoscale potentials from atomistic simulations. J Comput Chem 24(13):1624–1636. https://doi.org/10.1002/jcc.10307
7. Sovova Z, Berka K, Otyepka M, Jurecka P (2015) Coarse-grain simulations of skin ceramide NS with newly derived parameters clarify structure of melted phase. J Phys Chem B 119(10):3988–3998. https://doi.org/10.1021/jp5092366
8. Schulze E, Stein M (2018) Simulation of mixed self-assembled monolayers on gold: effect of terminal alkyl anchor chain and monolayer composition. J Phys Chem B 122(31):7699–7710. https://doi.org/10.1021/acs.jpcb.8b05075
9. Li Y, Kroger M, Liu WK (2011) Primitive chain network study on uncrosslinked and crosslinked cis-polyisoprene polymers. Polymer 52(25):5867–5878. https://doi.org/10.1016/j.polymer.2011.10.044
10. Li Y, Tang S, Abberton BC, Kroger M, Burkhart C, Jiang B, Papakonstantopoulos GJ, Poldneff M, Liu WK (2012) A predictive multiscale computational framework for viscoelastic properties of linear polymers. Polymer 53(25):5935–5952. https://doi.org/10.1016/j.polymer.2012.09.055
11. Li X, Kou D, Rao S, Liang H (2006) Developing a coarse-grained force field for the diblock copolymer poly (styrene-b-butadiene) from atomistic simulation. J Chem Phys 124(20):204909. https://doi.org/10.1063/1.2200694
12. Tschop W, Kremer K, Batoulis J, Burger T, Hahn O (1998) Simulation of polymer melts. I. Coarse-graining procedure for polycarbonates. Acta Polym 49(2-3):61–74. https://doi.org/10.1002/(sici)1521-4044(199802)49:2/3<61::aid-apol61>3.0.co;2-v
13. Agrawal V, Peralta P, Li YY, Oswald J (2016) A pressure-transferable coarse-grained potential for modeling the shock Hugoniot of polyethylene. J Chem Phys 145(10). https://doi.org/10.1063/1.4962255
14. Moore TC, Iacovella CR, McCabe C (2014) Derivation of coarse-grained potentials via multistate iterative Boltzmann inversion. J Chem Phys 140(22). https://doi.org/10.1063/1.4880555
15. Müller M, JJd P (2013) Computational approaches for the dynamics of structure formation in self-assembling polymeric materials. Annu Rev Mater Res 43(1):1–34. https://doi.org/10.1146/annurev-matsci-071312-121618
16. Salerno KM, Agrawal A, Perahia D, Grest GS (2016) Resolving dynamic properties of polymers through coarse-grained computational studies. Phys Rev Lett 116(5). https://doi.org/10.1103/PhysRevLett.116.058302
17. Salerno KM, Agrawal A, Peters BL, Perahia D, Grest GS (2016) Dynamics in entangled polyethylene melts. Eur Phys J-Spec Top 225(8-9):1707–1722. https://doi.org/10.1140/epjst/e2016-60142-7
18. Depa P, Chen CX, Maranas JK (2011) Why are coarse-grained force fields too fast? A look at dynamics of four coarse-grained polymers. J Chem Phys 134(1). https://doi.org/10.1063/1.3513365
19. Depa PK, Maranas JK (2005) Speed up of dynamic observables in coarse-grained molecular-dynamics simulations of unentangled polymers. J Chem Phys 123(9):94901. https://doi.org/10.1063/1.1997150
20. Lee H, de Vries AH, Marrink S-J, Pastor RW (2009) A coarse-grained model for polyethylene oxide and polyethylene glycol: conformation and hydrodynamics. J Phys Chem B 113(40):13186–13194. https://doi.org/10.1021/jp9058966
21. Nawaz S, Carbone P (2014) Coarse-Graining Poly (ethylene oxide)–Poly (propylene oxide)–Poly(ethylene oxide) (PEO–PPO–PEO) Block copolymers using the MARTINI force field. J Phys Chem B 118(6):1648–1659. https://doi.org/10.1021/jp4092249
22. Wu C (2019) Bulk modulus of poly(ethylene oxide) simulated using the systematically coarse-grained model. Comput Mater Sci 156:89–95. https://doi.org/10.1016/j.commatsci.2018.09.043
23. Brini E, Algaer EA, Ganguly P, Li C, Rodriguez-Ropero F, van der Vegt NFA (2013) Systematic coarse-graining methods for soft matter simulations - a review. Soft Matter 9(7):2108–2119. https://doi.org/10.1039/C2SM27201F
24. Lee H, Venable RM, MacKerell AD, Pastor RW (2008) Molecular dynamics studies of polyethylene oxide and polyethylene glycol: hydrodynamic radius and shape anisotropy. Biophys J 95(4):1590–1599. https://doi.org/10.1529/biophysj.108.133025
25. Martínez L, Andrade R, Birgin EG, Martínez JM (2009) PACKMOL: a package for building initial configurations for molecular dynamics simulations. J Comput Chem 30(13):2157–2164. https://doi.org/10.1002/jcc.21224
26. Agrawal V, Arya G, Oswald J (2014) Simultaneous iterative Boltzmann inversion for coarse-graining of polyurea. Macromolecules 47(10):3378–3389. https://doi.org/10.1021/ma500320n
27. Plimpton S (1995) Fast parallel algorithms for short-range molecular dynamics. J Comput Phys 117:1–19
28. Ruhle V, Junghans C, Lukyanov A, Kremer K, Andrienko D (2009) Versatile object-oriented toolkit for coarse-graining applications. J Chem Theory Comput 5(12):3211–3223. https://doi.org/10.1021/ct900369w
29. Humphrey W, Dalke A, Schulten K (1996) VMD: visual molecular dynamics. J Mol Graph Model 14(1):33–38
30. Alexander S (2010) Visualization and analysis of atomistic simulation data with OVITO–the open visualization tool. Model Simul

Mater Sc 18(1):015012. https://doi.org/10.1088/0965-0393/18/1/015012
31. van Zon A, Mos B, Verkerk P, de Leeuw SW (2001) On the dynamics of PEO-NaI polymer electrolytes. Electrochim Acta 46(10): 1717–1721. https://doi.org/10.1016/S0013-4686(00)00776-3
32. Wang QF, Keffer DJ, Nicholson DM (2011) A coarse-grained model for polyethylene glycol polymer. J Chem Phys 135(21). https://doi.org/10.1063/1.3664623
33. Choi E, Mondal J, Yethiraj A (2014) Coarse-grained models for aqueous polyethylene glycol solutions. J Phys Chem B 118(1):323–329. https://doi.org/10.1021/jp408392b
34. Taddese T, Carbone P (2017) Effect of chain length on the partition properties of (polyethylene oxide): comparison between MARTINI coarse-grained and atomistic models. J Phys Chem B 121(7):1601–1609. https://doi.org/10.1021/acs.jpcb.6b10858
35. Wu C (2018) Multiscale modeling scheme for simulating polymeric melts: application to poly(ethylene oxide). Macromol Theory Simul 27(1). https://doi.org/10.1002/mats.201700066
36. Chen CX, Depa P, Sakai VG, Maranas JK, Lynn JW, Peral I, Copley JRD (2006) A comparison of united atom, explicit atom, and coarse-grained simulation models for poly(ethylene oxide). J Chem Phys 124(23):234901. https://doi.org/10.1063/1.2204035
37. Cordeiro RM, Zschunke F, Mueller-Plathe F (2010) Mesoscale molecular dynamics simulations of the force between surfaces with grafted poly(ethylene oxide) chains derived from atomistic simulations. Macromolecules 43(3):1583–1591. https://doi.org/10.1021/ma902060k
38. Fischer J, Paschek D, Geiger A, Sadowski G (2008) Modeling of aqueous poly(oxyethylene) solutions: 1. Atomistic Simulations. J Phys Chem B 112(8):2388–2398. https://doi.org/10.1021/jp0765345
39. Chen QP, Xie S, Foudazi R, Lodge TP, Siepmann JI (2018) Understanding the molecular weight dependence of χ and the effect of dispersity on polymer blend phase diagrams. Macromolecules 51(10):3774–3787. https://doi.org/10.1021/acs.macromol.8b00604
40. Stubbs JM, Potoff JJ, Siepmann JI (2004) Transferable potentials for phase equilibria. 6. United-Atom Description for Ethers, Glycols, Ketones, and Aldehydes. J Phys Chem B 108(45): 17596–17605. https://doi.org/10.1021/jp049459w
41. Glotzer SC, Paul W (2002) Molecular and mesoscale simulation methods for polymer materials. Annu Rev Mater Res 32:401–436. https://doi.org/10.1146/annurev.matsci.32.010802.112213
42. Bayramoglu B, Faller R (2013) Modeling of polystyrene under confinement: exploring the limits of iterative Boltzmann inversion. Macromolecules 46(19):7957–7976. https://doi.org/10.1021/ma400831g
43. Huang H, Wu L, Xiong H, Sun H (2019) A transferrable coarse-grained force field for simulations of polyethers and polyether blends. Macromolecules 52(1):249–261. https://doi.org/10.1021/acs.macromol.8b01802
44. Xie ZM, Chai DL, Wang YS, Tan HF (2016) Directly modifying the nonbonded potential based on the standard iterative boltzmann inversion method for coarse-grained force fields. J Phys Chem B 120(45):11834–11844. https://doi.org/10.1021/acs.jpcb.6b06457
45. Enns JB, Simha R (2006) Transitions in semicrystalline polymers. II. Polyoxymethylene and poly(ethylene oxide). J Macromol Sci B 13(1):25–47. https://doi.org/10.1080/00222347708208751
46. Iwaoka N, Hagita K, Takano H (2018) Multipoint segmental repulsive potential for entangled polymer simulations with dissipative particle dynamics. J Chem Phys 149:114901. https://doi.org/10.1063/1.5046755
47. Sirk TW, Slizoberg YR, Brennan JK, Lisal M, Andzelm JW (2012) An enhanced entangled polymer model for dissipative particle dynamics. J Chem Phys 136(13):134903. https://doi.org/10.1063/1.3698476
48. Niedzwiedz K, Wischnewski A, Pyckhout-Hintzen W, Allgaier J, Richter D, Faraone A (2008) Chain dynamics and viscoelastic properties of poly(ethylene oxide). Macromolecules 41:4866–4872. https://doi.org/10.1021/ma800446n
49. Peters BL, Salerno KM, Agrawal A, Perahia D, Grest GS (2017) Coarse grained modeling of polyethylene melts: effect on dynamics. J Chem Theory Comput 13(6):2890–2896. https://doi.org/10.1021/acs.jctc.7b00241

Publisher's note Springer Nature remains neutral with regard to jurisdictional claims in published maps and institutional affiliations.